SAE TECHNICAL
PAPER SERIES

940909

Simulation of BioSID Head-Neck Motions

Devinder S. Grewal
Failure Analysis Associates, Inc.

Jacqueline G. Paver

Tara P. Khatua
Failure Analysis Associates, Inc.

**Reprinted from: Safety Technology
(SP-1041)**

SAE The Engineering Society For Advancing Mobility Land Sea Air and Space®
INTERNATIONAL

**International Congress & Exposition
Detroit, Michigan
February 28-March 3, 1994**

400 Commonwealth Drive, Warrendale, PA 15096-0001 U.S.A. Tel: (412)776-4841 Fax:(412)776-5760

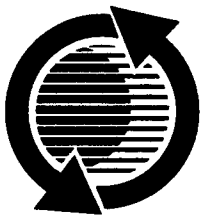

ISSN 0148-7191

Printed in USA 90-1203C/PG

940909

Simulation of BioSID Head-Neck Motions

Devinder S. Grewal
Failure Analysis Associates, Inc.

Jacqueline G. Paver

Tara P. Khatua
Failure Analysis Associates, Inc.

ABSTRACT

Numerous studies have been performed to develop and validate simulation data sets for adult frontal impact dummies; relatively few studies have been conducted for side impact dummies. This paper presents results of a study to develop and evaluate simulation parameters for the BioSID head-neck system.

The goal of this study was to review experimental data and develop, validate, and compare simulation parameters for the BioSID manikin head-neck system. BioSID is a state-of-the-art biofidelic side impact dummy recently developed by the Society of Automotive Engineers (SAE) for use in side impact tests to assess occupant protection. The BioSID head and neck are the same as the head and neck of the Hybrid III frontal crash test dummy. BioSID has been proposed as an alternative to the current side impact dummy, SID, required for side impact tests under Title 49 of the Code of Federal Regulations, Part 571.214.

The simulation parameters were derived from the literature and static, quasi-static, and dynamic lateral bending tests performed with BioSID necks. Simulations of the BioSID Head-Neck Pendulum (HNP) compliance tests were performed and different energy dissipation algorithms were studied. The simulation results were compared to response data from the HNP tests. It was found that while energy dissipation is required in any algorithm to produce dynamic stability, the choice of energy dissipation algorithm, whether it is viscous damping or differences in loading/unloading curves, does not materially affect the lateral head-neck response in this study. The results of this analysis will be useful in predicting the head and neck response of BioSID in side impacts.

INTRODUCTION

One aspect of automotive safety is occupant protection, and a valuable tool for evaluating safety system effectiveness and injury risk in real world accidents is crash testing using biofidelic anthropomorphic dummies. In order to reduce the cost of full-scale crash testing, simulations are also performed by mathematically modeling the dummy in the accident environment. A variety of mathematical models have been developed to predict biodynamic responses and injury potential. The prediction of injury requires accurate models of both the occupant and the accident environment.

Until recently, the bulk of modeling and crash testing efforts have focused on the adult frontal impact dummies; the development and use of side impact dummies is a relatively new concern. BioSID is a state-of-the-art dummy recently developed by the Society of Automotive Engineers (SAE) to assess occupant protection in side impacts. The BioSID head and neck are identical to the head and neck of the Hybrid III frontal crash test dummy developed by General Motors in 1976 (Beebe, 1990). BioSID has been proposed as an alternative to the current side impact dummy, SID, required for side impact tests under Title 49 of the Code of Federal Regulations, Part 571.214. The head-neck response of BioSID to lateral impact is considered superior to that of SID, and has been shown to be biofidelic (Seemann *et al.*, 1986).

Title 49 of the Code of Federal Regulations, Part 572 (49 CFR 572) gives specifications for the HNP compliance test for the Hybrid III frontal crash test dummy. The HNP compliance test and its performance standards for BioSID are similar to 49 CFR 572, and are designed to evaluate the head-neck assembly for adequate biofidelity and repeatability. The HNP compliance test is also useful in determining simulation parameters for the head and neck because its results provide head-neck response data to a very controlled and repeatable applied dynamic loading. This method has been used in previous studies to develop and evaluate simulation data sets for the Hybrid III head-neck in flexion and extension (Doherty and Paver, 1988; Paver *et al.*, 1990; Spittle *et al.*, 1992; Yang and Le, 1992).

In this study, the simulation parameters were first derived from the experimental literature (*i.e.* static, quasi-static, and dynamic lateral bending tests performed with BioSID and Hybrid III necks). Simulations of the HNP compliance test were performed with these parameters and they were tuned to produce adequate agreement between test and simulation

results. Three different energy dissipation algorithms were also studied to evaluate the relative merits of each.

The information generated by this study should serve as one step toward improving head and neck injury prediction potential. In particular, the proposed BioSID data set will be useful to researchers modeling experiments with this dummy. Ideally, these experiments and computer simulations will help us understand the responses of humans in side impacts.

BACKGROUND

The BioSID Head-Neck Structure – BioSID is a state-of-the-art biofidelic anthropomorphic side impact dummy. Figure 1 is a side view of the head and neck. The head is a hollow two-piece casting of 356-T6 aluminum with vinyl skin cover. The molded neck is a segmented flexible member constructed of alternate layers of aluminum and butyl rubber discs. Since the rubber discs are asymmetric, the neck exhibits different mechanical responses in flexion, extension, and lateral bending. Aluminum plates molded into each end of the neck provide attachments to the head and pendulum. A load cell, mounted in the head, attaches the head to the neck. Rubber nodding blocks are mounted at the head-neck joint to simulate the flexion and extension responses of the human occipital condyle joint. A steel cable, which runs through the center of the neck, provides axial strength. The base of the neck is rigidly attached to the pendulum by a bracket adjustable in the sagittal plane.

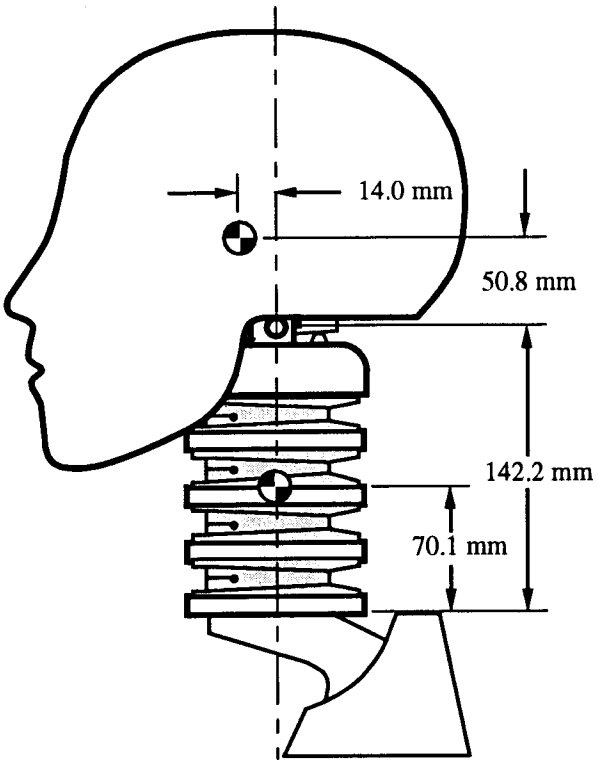

Figure 1. BioSID Head-Neck Complex. Dimensions are from experimental measurements (Kaleps and Whitestone, 1988).

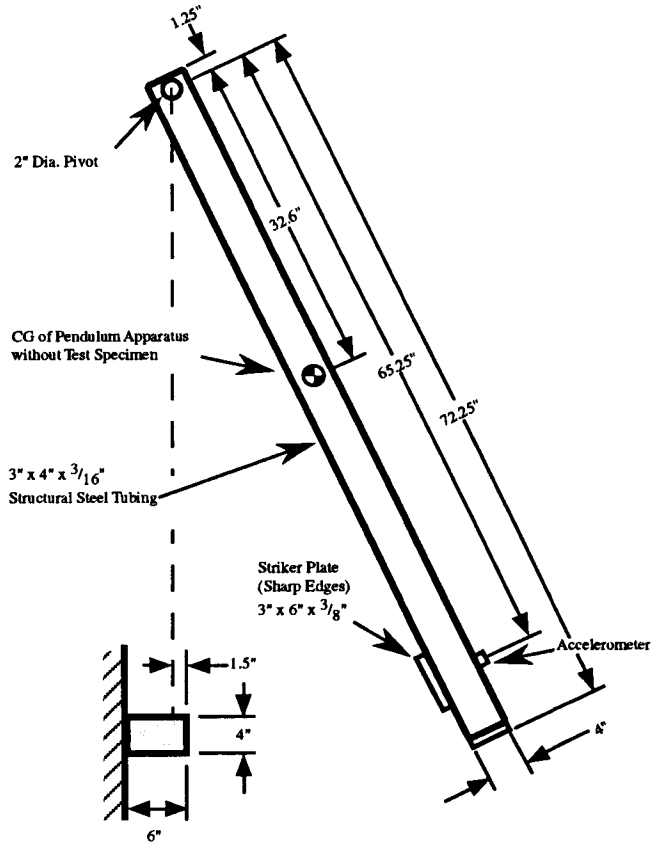

Figure 2. Head-Neck Pendulum Test Apparatus (*User's Manual for the BioSID Side Impact Dummy* 1991).

The Head-Neck Pendulum Test – The HNP test measures the dynamic response of the head and neck to a specified lateral pendulum deceleration; compliance with performance standards is designed to ensure that the response of the head-neck structure is biofidelic and repeatable. The BioSID head-neck calibration test apparatus (Figure 2), instrumentation requirements, environmental conditions, protocol, and performance standards are specified in the *User's Manual for the BioSID Side Impact Dummy* (1991).

The HNP test consists of a pendulum dropped from an initial angle such that the accelerometer location, which travels in a circular path of radius r = 1.657 m, has a specified tangential impact speed of 6.89 to 7.13 m/s. At the bottom of the pendulum's swing, the arm impacts a block of honeycomb, which produces a specified near square wave pendulum deceleration pulse. The head-neck system, which is mounted to the end of the pendulum, undergoes no impact.

The performance standards specify the BioSID head-neck response, after pendulum-honeycomb contact, by the following parameters:

- Total head rotation relative to the pendulum vs. time (HP Rotation)
- Moment about the occipital condyles vs. time. (HN Moment)

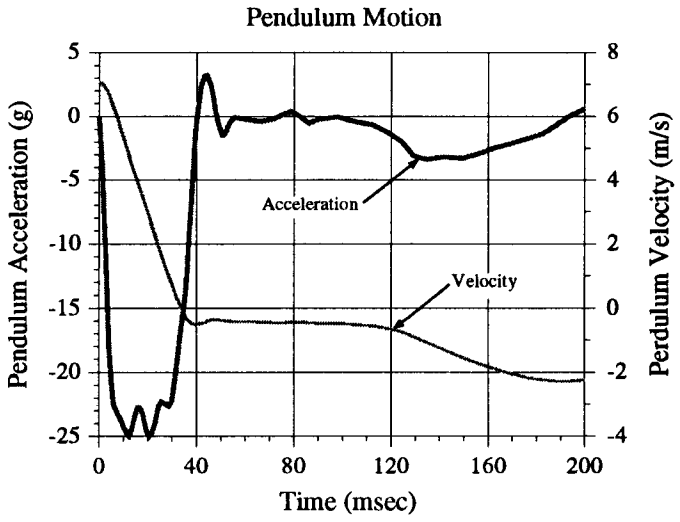

Figure 3. Motion of the pendulum measured at the accelerometer mounting location. The pendulum striker plate contacts the honeycomb at time = 0. The pendulum velocity is obtained by integrating the measured acceleration pulse. Velocity at time of impact was 7.06 m/s.

For this study, HNP test data was provided by First Technology Safety Systems, Inc., one of the developers of BioSID. The tests were conducted on BioSID necks #1303 and #1356. The total of four HNP tests were in agreement within 3% in both pendulum acceleration and head-neck response, and data from one representative test was chosen for the simulations. Figure 3 shows the measured pendulum acceleration and velocity at the accelerometer mounting location for the representative test. These are the data used to specify the motion of the pendulum in the simulations.

SIMULATION FORMULATION

The Model – The decision to derive a model from first principles was motivated by the desire to model the test conditions as accurately as possible so that the effects of individual parameters could be better determined. The equations of motion are written so that the measured pendulum acceleration can be applied directly to the model to specify the motion of the pendulum.

In order to make the results of this study applicable to the existing occupant dynamics simulation programs such as ATB* and MADYMO**, the HNP test system is modeled as a planar rigid body system. The continuously flexible neck of BioSID is approximated as a rigid body with pin joints at the base of the neck (NP joint) and at the occipital condyles (HN joint). This rigid body formulation is shown schematically in Figure 4. The stiffness and viscoelastic properties of the neck are incorporated into these two joints.

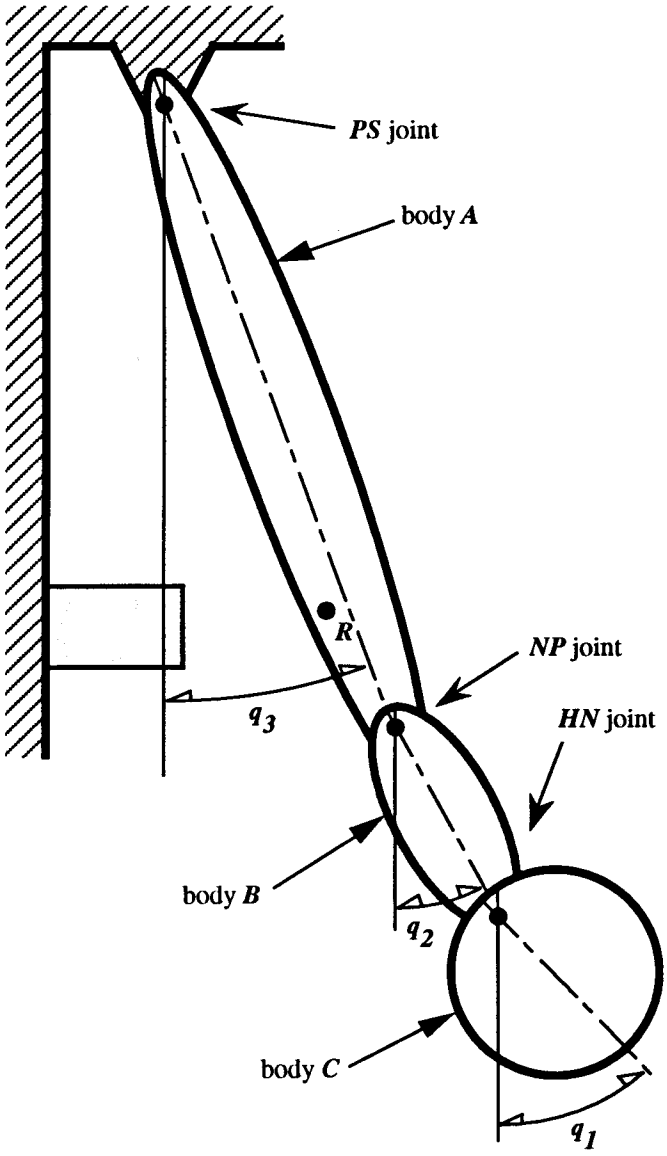

Figure 4. Rigid Body Formulation of HNP Test System

The equations of motion for this system were formulated by Kane's method (Kane and Levinson, 1985). AUTOLEV was used to perform the kinematics, develop the equations of motion, and write the FORTRAN code for solving the equations of motion. AUTOLEV is a symbol manipulator (available from Online Dynamics in Sunnyvale, California) used to aid in developing equations of motion and code for solving them. A fourth-order predictor-corrector integration procedure based on the Kutta-Merson method is used to numerically integrate the equations of motion. The Checking Function (Kane and Levinson, 1992) was used to check the results of the integration. The Checking Function is a type of energy integral that should remain constant if the equations of motion are valid and the integration is properly carried out.

* Articulated Total Body (ATB) is a crash victim simualtion code maintained by Armstrong Aerospace Medical Research Laboratory, Wright-Patterson Air Force Base, Ohio.

** MADYMO is a crash victim simulation code developed by TNO Road Vehicles Research Institute, Delft, The Netherlands.

The basis of the mathematical formulation of the model and the equations of motion are presented in Appendix B.

The most general algorithm for computing joint resistive torques in this study has nine parameters; three parameters for the bilinear loading curve that passes through the origin and is symmetric about the origin, four parameters for the bilinear unloading curve that does not necessarily pass through the origin but is symmetric about the origin, one parameter for the hysteresis slope that connects the loading curve to the unloading curve, and one parameter for the viscous damping torque. As the joint is loaded the torque is computed along the loading curve. When unloading occurs (*i.e.* the sign of the relative angular velocity between bodies is different from the sign of the relative angle between bodies), the torque is computed along the hysteresis slope until it intersects the unloading curve. The unloading slope is used until a loading condition is again detected.

By varying the above nine parameters, a variety of joint torque algorithms can be studied; ranging from a simple linear algorithm with no energy dissipation to a complex algorithm with different loading and unloading curves.

Model Validation – The results of the integration of the equations of motion were validated using the Checking Function. It remained constant for all simulations, but did show small oscillations during the first 10 milliseconds of all simulations, probably because the specified deceleration is not smooth at t_o.

The equations of motion and the computer code were verified by duplicating simulations performed by another independent model. Paver *et al.*, (1990) conducted similar HNP simulations for flexion and extension using ATB. The inertia data and joint stiffnesses proposed by the Armstrong Aerospace Medical Research Laboratory (AAMRL) for the Hybrid III 50th percentile male dummy were incorporated into the subject model and the head-neck responses (i.e. HP rotation and HN moment) were compared with those given in the report. The agreement of both simulations indicates consistency between ATB and the subject model.

EXPERIMENTAL DATA FOR BIOSID NECK LATERAL STIFFNESS

The experimental data about lateral neck stiffness was used to as a starting point to derive the simulation parameters. These parameters were then tuned to produce agreement between test responses and simulations.

Static stiffness data is usually obtained by measuring the moment-rotation curve of the neck subjected to lateral bending. Since the neck is similar to an elastic beam, the moment is measured at one end and the rotation is taken to be the difference in angle between the two ends of the neck. Table 1 summarizes the available stiffness data for the Hybrid III head-neck structure which is the same as the BioSID head and neck.

Baughn *et al.* (1992, 1993) measured the static loading and unloading curves of the Hybrid III neck in lateral flexion. Their data shows that the static stiffness is approximately linear for head rotations less than 65°. Kaleps *et al.* (1988) measured the static loading stiffness and also calculated the dynamic loading stiffness and viscous damping factor by spectral methods. They found the damping factor (ratio of damping to critical damping) to be approximately 0.2. For this study the critical damping was calculated by approximating the head and neck as a single degree-of-freedom spring-mass-damper system. For a single DOF system, the critical damping is two times the square root of the product of stiffness and moment of inertia. For this calculation, the stiffness under dynamic loading was given and the moment of inertia was approximated using the inertia of the head about both neck joints as bounding values. Using data from Kaleps *et al.* (1988), the range of inertias was calculated to be 5-13 kg-m^2 and the stiffness was given as 4.1 N-m/deg. This yields a critical damping of 0.16 N-m-s/deg. Using a damping ratio of 0.2 we get a damping factor of 0.032 N-m-s/deg. This value was used a starting point in the simulations.

Table 1. BioSID Neck Lateral Stiffness Data

Condition	Lateral Stiffness (N-m/deg)	Source
Static Loading	2.1	Baughn *et al.*, 1993
Static Unloading	1.4 - 1.6	
Static Loading	2.8 - 3.2	Kaleps *et al.*, 1988
Dynamic Loading	4.0 - 4.2	

SIMULATIONS

Four different simulations were performed, each with increasing complexity of energy dissipation algorithm. The joint stiffness algorithm for each simulation are summarized in Figure 5. It was assumed that the head-neck and neck-pendulum joints in the rigid body model are identical so that the same joint algorithm is applied to both joints.

Simulations were performed of the impact phase, where time t_o was the time of initial contact of the pendulum with the honeycomb block. The applied deceleration pulse was digitized from the measured acceleration time history and numerically integrated to obtain the velocity. At time t_o, bodies *A, B,* and *C* (Figure 4) are located at an angle of 3.44 deg with respect to the vertical, the tangential impact speed of point *R* on body *A* is 7.06 m/s which corresponds to an angular velocity for body *A* of 244 deg/s.

In each simulation, the joint algorithm parameters were varied to investigate their effects on the response (HP rotation and HN moment), and the parameters were adjusted to match simulation results to test results.

Algorithm for Simulation 1:

Linear static joint stiffness; no energy dissipation; unloading stiffness is the same as the linear loading stiffness.

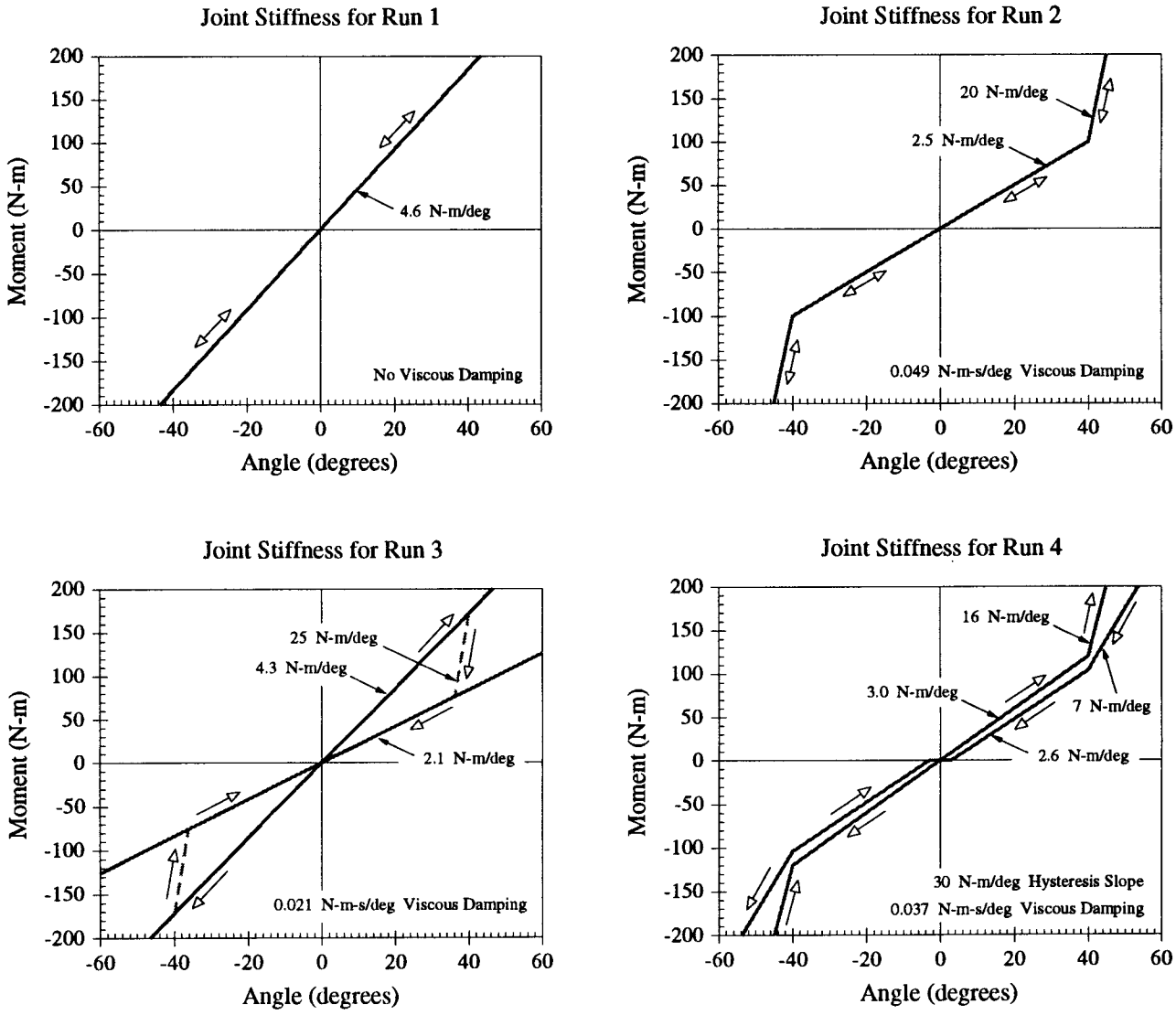

Figure 5. Summary of the different static joint stiffness models applied to both HN and NP joints for each run.

Algorithm for Simulation 2:

Bilinear static joint stiffness; viscous damping both during loading and unloading; unloading stiffness is the same as the loading stiffness.

Algorithm for Simulation 3:

Linear static joint stiffness for loading; linear unloading stiffness less than the loading stiffness; Hysteresis slope for going from loading to unloading curves; viscous damping.

Algorithm for Simulation 4:

Most general model – Bilinear static joint stiffness for loading; bilinear unloading stiffness less than the loading stiffness (not necessarily passing through the origin); Hysteresis slope for going from loading to unloading curves; viscous damping.

RESULTS

The adjusted parameters for each joint stiffness model are given in Figure 5. The same model were applied to both joints. Plots of the results of each simulation run are given in Appendix A along with the experimental test data.

In simulation 1, the joint stiffnesses were assumed to be functions of the joint rotation angle only. Variations in the joint stiffness affected the timing and magnitude of the peak HP rotation; higher stiffnesses produced lower rotation peaks which occurred sooner. A joint stiffness of 4.6 N-m/deg gives the best compromise between the timing and magnitude of the first peak HP rotation. This model shows a high degree of dynamic instability, evidenced by the oscillations in the HN moment and the crossing-over of the moment rotation curve.

In simulation 2, two refinements were made; viscous damping was added, which lowered the peak joint rotations and produced decay in the overall response of both the total head rotation and the HN moment, and a bilinear joint stiffness was used to better capture the non-linear behavior of the neck at higher deflections. The viscous damping also created stability (i.e., the loading path did not intersect the unloading path in the moment-rotation curve) and a time lag between the rotation and HN moment. The damping was adjusted to lower the peaks and give the best compromise between stability and the timing of peaks. Best results were obtained with a damping ratio of 0.049 N-m-s/deg and a bilinear static joint stiffness of 2.5 N-m/deg and 20 N-m/deg with the change in slope occurring at 40 degrees of joint rotation

In simulations 3 and 4, energy dissipation was modeled using viscous damping and hysteresis (i.e. different static loading and unloading curves). The addition of hysteresis did not produce significantly different results from simulation 2, although some of the kinks in the HN moment curve were better reproduced. The values used for the best fit between test and simulation are shown on the charts in Figure 5.

CONCLUSIONS

Based on the results of the simulations performed in this study, the following conclusions are warranted:

- Energy dissipation is required in any reasonable model to create dynamic stability.
- The choice of energy dissipation algorithm does not appear to materially affect the results.
- The bilinear stiffness model with viscous damping (simulation 2) is to be preferred over more complex algorithms because it produces similar results without the added complexity.
- Further study needs to be done with greater pendulum velocities that create head-neck excursions into highly non-linear regions.

Acknowledgments – The authors wish to thank Gerry Locke at First Technology Safety Systems, Inc. for providing the HNP test data used in these simulations. The senior author would also like to extend his gratitude to professors Tom Kane and David Levinson of Stanford University for teaching the theory *and practice* of dynamics.

REFERENCES

1. Baughn, D.J., Spittle, E.K., Thompson, G., "A New Technique for Determining Bending Stiffness of Mechanical Necks," SAE Paper #930099, *Human Surrogates: Design, Development & Side Impact Protection*, February 1993.
2. Beebe, M.S., "What is Biosid?," SAE Paper #900377, 1990.
3. Doherty, B.J. and Paver, J.G., "Mathematical Modeling of the Hybrid III Manikin Head-Neck Structure," *Proceedings of the International Conference on Mathematical Modeling*, 1988.
4. Foster, J.K., Kortge, J.O., and Wolanin, M.J., "Hybrid III – A Biomechanically-Based Crash Test Dummy," SAE Paper #770938, *Proceedings of the Twenty-First Stapp Car Crash Conference*, October 1977.
5. Kaleps, I., White, R.P., Beecher, R.M., Whitestone, J. and Oberglfell, L.A., Hybrid III Geometrical and Inertial Properties and Analytical Simulation Data Base Development," Armstrong Aerospace Medical Research Laboratory, Wright-Patterson Air Force Base, Ohio, Report #AAMRL-TR-88-005, February 1988.
6. Kaleps, I. and Whitestone, J., "Measurement of Hybrid III Dummy Properties," SAE Paper #880638, 1988.
7. Kane, T.R. and Levinson, D.A., *Dynamics Online*. 1992.
8. Kane, T.R. and Levinson, .D.A., *Dynamics: Theory and Applications*. McGraw-Hill, 1985.
9. *Motor Vehicle Safety Standard No. 208: Occupant Crash Protection*. Title 49, Code of Federal Regulations, Part 571.208, 1992.
10. *Motor Vehicle Safety Standard No. 214: Side Impact Protection*. Title 49, Code of Federal Regulations, Part 571.214, 1992.
11. *National Highway Traffic Safety Administration Regulations on Anthropomorphic Test Dummies*. Title 49, Code of Federal Regulations, 572, 1992.
12. Paver, J.G., Khatua, T.P., Piziali, R.L., Whitestone, J., Kaleps, I. and Taylor, C., "The Prediction of Hybrid III Manikin Head-Neck Kinematics and Dynamics," SAE Paper #900540, 1990.
13. Seemann, M.R., Muzzy III, W.H., Lustick, L.S., "Comparison of Human and Hybrid III Head and Neck Dynamic Response," SAE Paper #861892, 1986.
14. Spittle, E.K., Shipley, B.W. Jr., Kaleps, I. and Miller, D.J., "Hybrid II and III Dummy Neck Properties for Computer Modeling," Armstrong Aerospace Medical Research Laboratory, Wright-Patterson Air Force Base, Ohio, Report #AL-TR-1992-0049, February 1992.
15. *User's Manual for the BioSID Side Impact Dummy*, Society of Automotive Engineers, Dummy Testing Equipment Subcommittee, Engineering Aid 24, April, 1991.
16. Yang, K.H. and Le, J., "Finite Element Modeling of Hybrid III Head-Neck Complex," SAE Paper #922526, *Proceedings of the Thirty-Sixth Stapp Car Crash Conference*, November 1992.

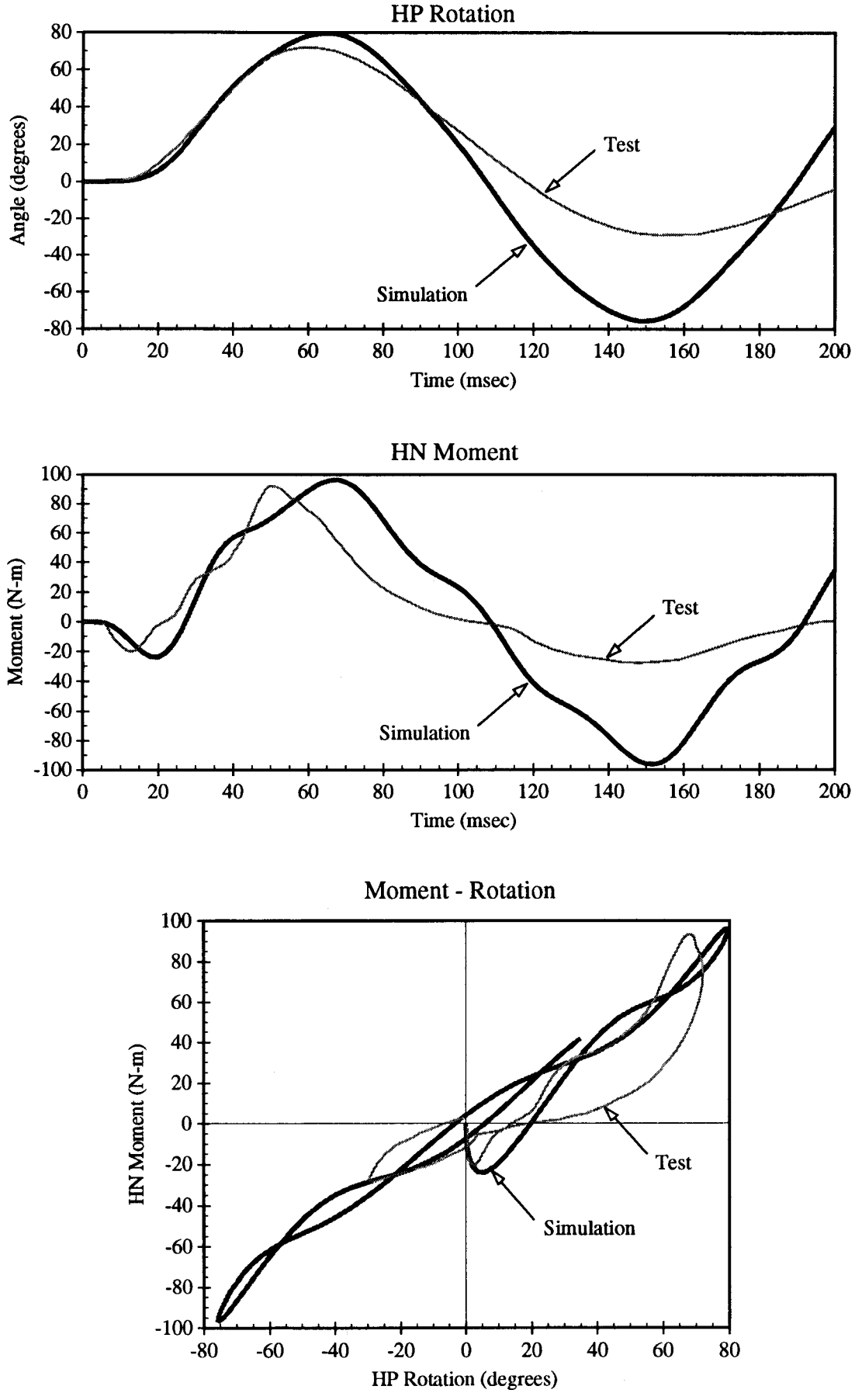

Figure 6. Comparison of test data with results of simulation run 1 – no energy dissipation

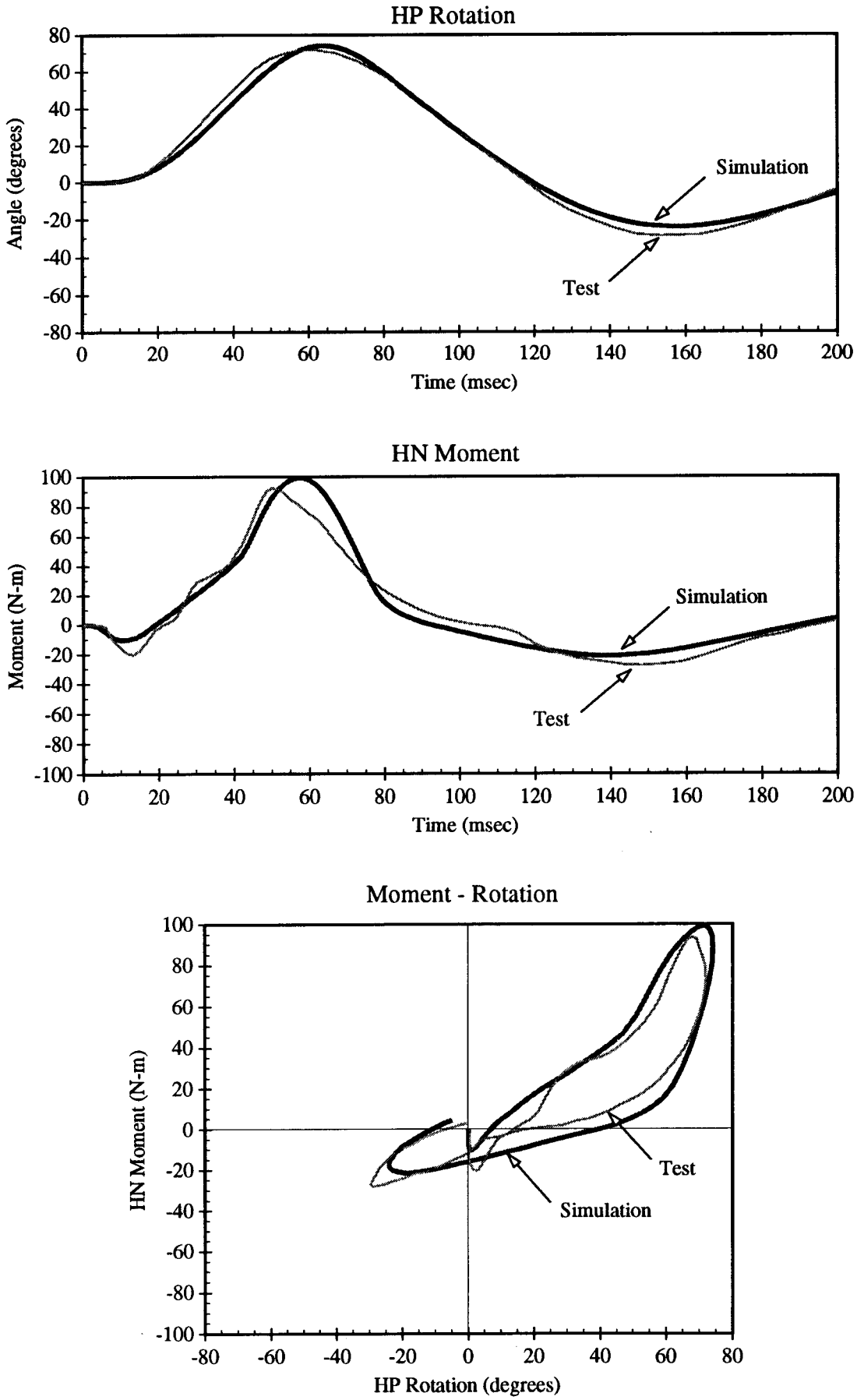

Figure 7. Comparison of test data with results of simulation run 2 – viscous damping only

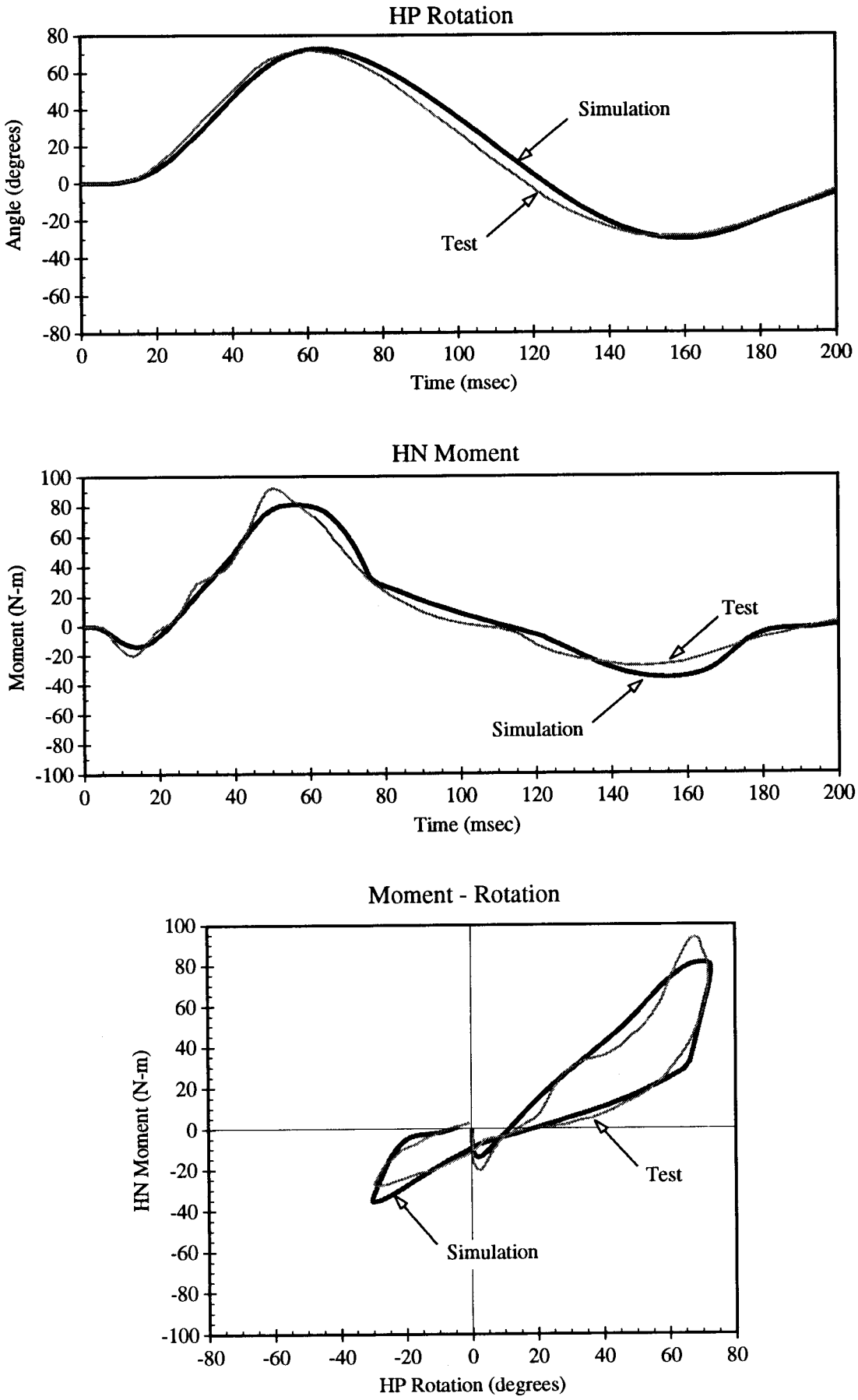

Figure 8. Comparison of test data with results of simulation run 3 – viscous damping with hysteresis model 1

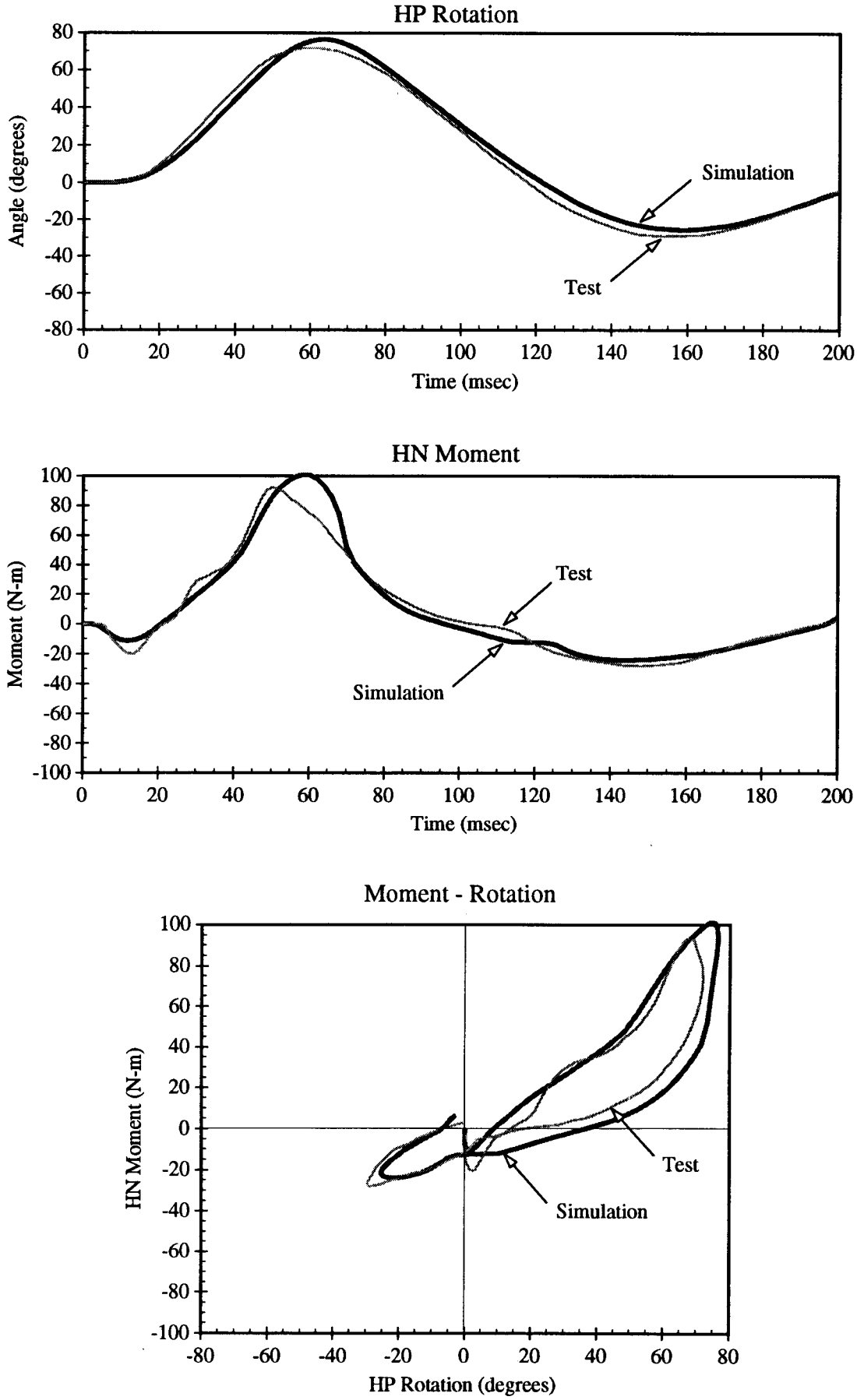

Figure 9. Comparison of test data with results of simulation run 4 – viscous damping with hysteresis model 2

APPENDIX B – Development of Simulation Model

Figure 10 shows a planar system S formed by three pin connected rigid bodies: *A*, *B* and *C*. Body *A* is pinned in a Newtonian reference frame *N* at a point *O* fixed in both *A* and *N*. Body *B* is pinned to *A* at a point *P* fixed in both *A* and *B*. And, body *C* is pinned to body *B* at a point *Q* fixed in both *B* and *C*. Points *A**, *B** and *C** are the mass centers of bodies *A*, *B* and *C* respectively. Bodies *A*, *B* and *C* are oriented in *N* by simple right-handed rotation about points *O*, *P* and *Q* respectively. The rotations are characterized by the angles q_3 q_2 and q_1 respectively measured from the vertical to a line fixed on the body. Since the motion of *A* is specified, *S* possesses two degrees of freedom in *N*; the associated generalized speeds are:

$$u_i = \dot{q}_i \quad (i = 1,2) \tag{1}$$

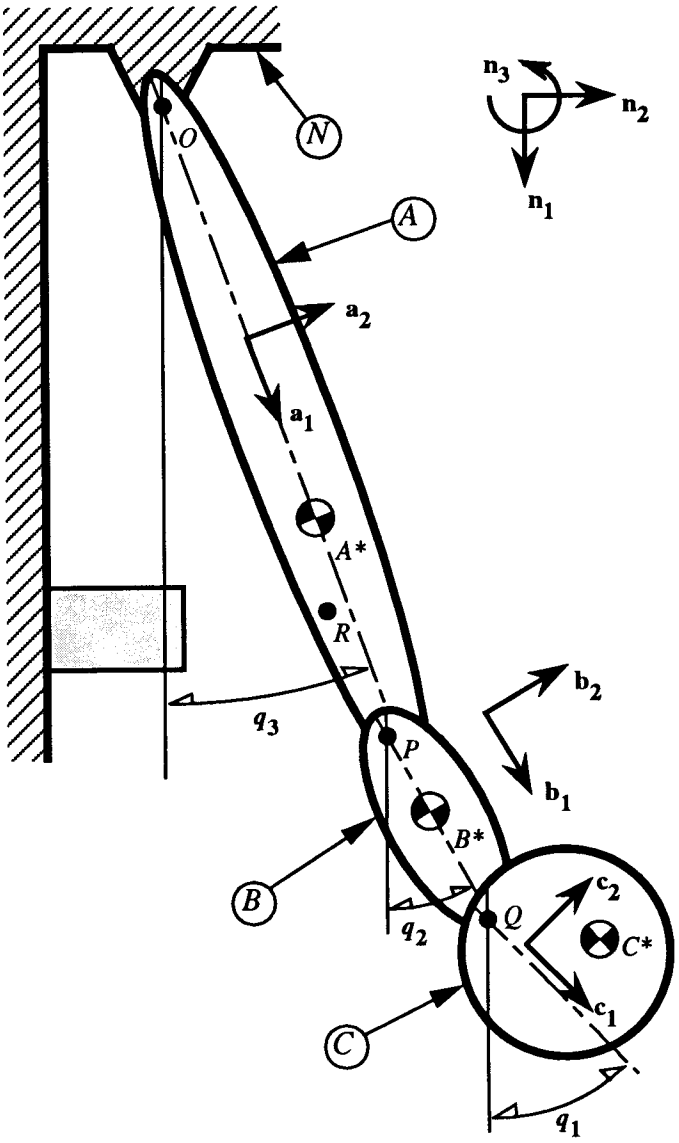

Figure 10. Schematic of Dynamical System

The moments of inertia of bodies *A*, *B* and *C* about the mass centers in the direction of $\mathbf{n_3}$ are J_A, J_B and J_C respectively. The position vectors describing the location of the points are defined as follows:

$$\begin{aligned}
\mathbf{p}^{OA*} &= l_1\mathbf{a_1} + l_2\mathbf{a_2} \\
\mathbf{p}^{OR} &= l_3\mathbf{a_1} + l_4\mathbf{a_2} \\
\mathbf{p}^{OP} &= l_5\mathbf{a_1} + l_6\mathbf{a_2} \\
\mathbf{p}^{PB*} &= l_7\mathbf{b_1} + l_8\mathbf{b_2} \\
\mathbf{p}^{PQ} &= l_9\mathbf{b_1} + l_{10}\mathbf{b_2} \\
\mathbf{p}^{QC*} &= l_{11}\mathbf{c_1} + l_{12}\mathbf{c_2}
\end{aligned} \tag{2}$$

the position vectors are expressed as generally as possible so that flexion and extension tests can be simulated, in addition to this lateral flexion test, by changing the configuration of the system at the time the simulation is actually performed.

The set of all contact and distance forces applied to the system *S* (joint resistive torques and gravity) can be replaced by a single force applied at each mass center of bodies *B* and *C* in the $\mathbf{n_1}$ direction, and torques applied to body *B* and *C* in the $\mathbf{n_3}$ direction:

$$\begin{aligned}
\mathbf{F}^{B*} &= m_B g\mathbf{n_1} \\
\mathbf{F}^{C*} &= m_C g\mathbf{n_1} \\
\mathbf{T}^{A/B} &= NP\mathbf{n_3} \\
\mathbf{T}^{B/C} &= HN\mathbf{n_3}
\end{aligned} \tag{3}$$

where *g* is the acceleration due to gravity, m_B and m_C are the masses of body *B* and *C* respectively, and *NP* and *HN* are the measure numbers of the resistive torques generated at the neck-pendulum and head-neck joints respectively. These torques are functions of joint rotation (stiffness), direction of rotation (hysteresis), and rotation speed (damping).

The equations of motion are formulated with the aid of AUTOLEV using Kane's method (Kane and Levinson, 1985 & 1992). Both the dynamical and kinematical equations of motion are given below.

kinematical:

$$\begin{aligned}
u_1 &= \dot{q}_1 \\
u_2 &= \dot{q}_2 \\
\Omega &= \dot{q}_3
\end{aligned} \tag{4}$$

dynamical:

$$\mathbf{X}\dot{\mathbf{u}} = \mathbf{Y} \quad \Leftrightarrow \quad \begin{bmatrix} X_{11} & X_{12} \\ X_{21} & X_{22} \end{bmatrix} \begin{Bmatrix} \dot{u}_1 \\ \dot{u}_2 \end{Bmatrix} = \begin{Bmatrix} Y_1 \\ Y_2 \end{Bmatrix} \tag{5}$$

$$
\begin{aligned}
X_{11} &= -(l_{11}^2 + l_{12}^2)m_C - J_C \\
X_{12} = X_{21} &= -[(l_{10}l_{12} + l_{11}l_9)\cos(q_1 - q_2) \\
&\quad +(l_{10}l_{11} - l_9 l_{12})\sin(q_1 - q_2)]m_C \\
X_{22} &= -(l_{10}^2 + l_9^2)m_C - (l_7^2 + l_8^2)m_B - J_B
\end{aligned} \tag{6}
$$

$$
\begin{aligned}
Y_1 &= \{u_2^2[(l_9 l_{12} - l_{10}l_{11})\cos(q_1 - q_2) \\
&\quad +(l_9 l_{11} - l_{10}l_{12})\sin(q_1 - q_2)] \\
&\quad +\cos(q_1 - q_3)[(l_{11}l_5 + l_{12}l_6)\dot{\Omega} + (l_{12}l_5 - l_{11}l_6)\Omega^2] \\
&\quad +\sin(q_1 - q_3)[(l_{11}l_6 - l_{12}l_5)\dot{\Omega} + (l_{11}l_5 + l_{12}l_6)\Omega^2] \\
&\quad +g(l_{12}\cos q_1 + l_{11}\sin q_1)\}m_C + HN \\
Y_2 &= \{u_1^2[(l_{10}l_{11} - l_9 l_{12})\cos(q_1 - q_2) \\
&\quad -(l_{10}l_{12} + l_9 l_{11})\sin(q_1 - q_2)] \\
&\quad +\cos(q_2 - q_3)[(l_6 l_{10} + l_5 l_9)\dot{\Omega} + (l_5 l_{10} - l_6 l_9)\Omega^2] \\
&\quad +\sin(q_2 - q_3)[(l_6 l_9 - l_5 l_{10})\dot{\Omega} + (l_6 l_{10} + l_5 l_9)\Omega^2] \\
&\quad +g(l_{10}\cos q_2 + l_9 \sin q_2)\}m_C \\
&\quad +\{\cos(q_2 - q_3)[(l_5 l_7 + l_6 l_8)\dot{\Omega} + (l_5 l_8 - l_6 l_7)\Omega^2] \\
&\quad +\sin(q_2 - q_3)[(l_6 l_7 - l_5 l_8)\dot{\Omega} + (l_5 l_7 + l_6 l_8)\Omega^2] \\
&\quad +g(l_8\cos q_2 + l_7 \sin q_2)\}m_B + HN - NP
\end{aligned} \tag{7}
$$

In order to specify the motion of body A in N, the angular velocity of A in N, $\left({}^N\omega^A = \Omega \mathbf{a}_3\right)$, and a compatible angular acceleration of A in N, $\left({}^N\alpha^A = \dot{\Omega}\mathbf{a}_3\right)$, is needed. If A (the pendulum) is assumed to be slender, then the information recorded during the HNP test can be numerically integrated to provide $\dot{\Omega}$ and Ω.

$$
\begin{aligned}
\dot{\Omega} &= \frac{y}{r} \\
\Omega &= \omega_o + \frac{1}{r}\int_{t_o}^{t} y\,dt
\end{aligned} \tag{8}
$$

where ω_o is the measured speed of point R (the accelerometer mounting point) at the time of impact, and y is the measured tangential acceleration of point R.

Parameters for lateral HNP test – In a lateral flexion head-neck pendulum test for the BioSID, the pendulum (body A) is dropped from an initial angle such that point R has a tangential speed at impact specified to be between 6.89 and 7.13 m/s. Point R travels on a circular path of radius r, and r is specified to be 1.657 m. From these test specifications the initial angular velocity of bodies A, B and C is between -4.157 and 4.302 rad/s. Impact occurs at t=0 when the body A contacts the aluminum honeycomb block. At the point of contact, the width of the pendulum and the size of the honeycomb block create an initial angle for bodies A, B and C of q_3=q_2=q_1=3.44 deg (=060 radians).

The geometry of the pendulum, as shown in Figure 2, provides values for l_1 to l_6 as follows:

$$
\begin{aligned}
l_1 &= 0.828 \text{ m} \\
l_2 &= 0.0 \\
l_3 &= 1.657 \text{ m} \\
l_4 &= -0.051 \text{ m} \\
l_5 &= 1.905 \text{ m} \\
l_6 &= 0.0762 \text{ m}
\end{aligned} \tag{9}
$$

The mass and inertia of the pendulum are given in the test specifications (*User's Manual for the BioSID Side Impact Dummy*, 1991) to be:

$$
\begin{aligned}
m_A &= 29.6 \text{ kg} \\
J_A &= 12.95 \text{ kg}\cdot\text{m}^2
\end{aligned} \tag{10}
$$

But, they do not appear explicitly in the equations of motion since the motion of the pendulum is specified.

The dimensions of the head and neck, the locations of the mass centers, masses, and appropriate inertias are obtained from measurements made of the Hybrid III dummy (Kaleps and Whitestone, 1988; and Kaleps et al., 1988):

$$
\begin{aligned}
l_7 &= 0.070 \text{ m} \\
l_8 &= 0.0 \\
l_9 &= 0.140 \text{ m} \\
l_{10} &= 0.0 \\
l_{11} &= 0.051 \text{ m} \\
l_{12} &= 0.0 \\
m_B &= 1.210 \text{ kg} \\
m_C &= 4.498 \text{ kg} \\
J_B &= 0.0029 \text{ kg}\cdot\text{m}^2 \\
J_C &= 0.0159 \text{ kg}\cdot\text{m}^2
\end{aligned} \tag{11}
$$